Fusion of the weakly bound projectile ^{9}Be with ^{89}Y

C. S. Palshetkar,[1] S. Santra,[1,*] A. Chatterjee,[1] K. Ramachandran,[1] Shital Thakur,[2] S. K. Pandit,[1] K. Mahata,[1] A. Shrivastava,[1] V. V. Parkar,[2,†] and V. Nanal[2]

[1]*Nuclear Physics Division, Bhabha Atomic Research Centre, Mumbai 400 085, India*

[2]*Department of Nuclear and Atomic Physics, Tata Institute of Fundamental Research, Mumbai 400 005, India*

(Received 20 August 2010; published 19 October 2010)

The excitation function for the complete fusion of ^{9}Be + ^{89}Y has been measured at near-barrier energies, and the barrier distribution has been extracted from the fusion data. Coupled-channels calculations have been carried out to understand the effect of coupling of both the projectile and target excitations on the above quantities. The complete fusion cross sections, especially at above-barrier energies, have been found to be suppressed by (20 ± 5)% compared to the ones predicted by the coupled-channels calculations that do not include the couplings to the projectile continuum, indicating the loss of flux from the entrance channel before fusion. This conclusion is also supported by a considerable incomplete fusion cross section observed for this system. Fusion measurements for two more systems have been carried out, namely, for ^{4}He + ^{93}Nb and ^{12}C + ^{89}Y, which involve tightly bound projectiles and form compound nuclei nearby to that formed in ^{9}Be + ^{89}Y fusion. Comparison of the fusion data obtained for all three systems further confirms the suppression of complete fusion in the ^{9}Be + ^{89}Y system. Systematics of the suppression factor observed for ^{9}Be induced fusion in different mass targets is discussed.

DOI: 10.1103/PhysRevC.82.044608 PACS number(s): 25.70.Jj, 25.70.Gh

I. INTRODUCTION

Fusion reactions with weakly bound projectiles are interesting because of their importance in astrophysical reactions, namely, in understanding the nucleosynthesis process and in studying nuclei near the drip lines. Weakly bound nuclei exhibit properties such as low breakup threshold due to low binding energy per nucleon and thus have very few or no bound excited states, larger rms radii compared to the value obtained from systematics ($R = r_o A^{1/3}$), larger transfer probability, etc. Due to their low breakup threshold, the effect of breakup coupling to different reaction channels is expected to be important. To investigate this, reactions with weakly bound unstable projectiles have been carried out due to the recent availability of radioactive ion beams (RIBs), however, with low beam intensities and thus poor statistics. Hence, reactions induced by weakly bound stable projectiles become important as good quality data can be obtained, and comparison of different reaction quantities measured for reactions induced by both weakly bound stable and unstable nuclei becomes possible.

Due to the finite probability of projectile breakup, fusion induced by weakly bound projectiles can lead to two distinct processes: complete fusion (CF), in which the whole projectile fuses with the target, and incomplete fusion (ICF), in which part of the projectile fuses with the target. There have been many experimental investigations to study the effect of breakup on fusion with weakly bound stable ^{6,7}Li and ^{9}Be as well as unstable projectiles like ^{6,8}He and ^{7,10,11}Be [1–9]. In the case of fusion of the stable weakly bound projectiles with heavy mass targets, a general observation of ∼30% suppression of the CF cross sections, compared to the coupled-channels (CC) calculations, has been reported at above-barrier energies. On the other hand, for reactions with the light mass targets, the CF cross sections as obtained in Ref. [10] do not show any suppression. In the case of fusion of weakly bound unstable nuclei, it has been observed that even the total fusion (TF) cross sections at above-barrier energies are suppressed compared to the one-dimensional barrier penetration model calculations (1D-BPM). Theoretical calculations carried out for ^{6,8}He [2] induced fusion reactions suggest that the suppression observed could be due to the importance of coupling of neutron transfer channels at these energies. From studies with tightly bound nuclei, it has been established that the coupling of the relative motion of the colliding nuclei to different reaction channels leads to enhancement of fusion cross sections at subbarrier energies [11,12]. Coupled-channels calculations performed for the ^{11}Be + ^{208}Pb system [13] show that coupling to the breakup channel leads to suppression above barrier and enhancement below the barrier compared to the 1D-BPM values. However, *a priori* estimates of enhancement or suppression for reactions induced by weakly bound nuclei cannot be made, because their breakup leads to the coupling of reaction channels to continuum states.

In the case of fusion reactions induced by ^{9}Be, CF suppressions of ∼32% for ^{9}Be + ^{208}Pb [14] and ^{9}Be + ^{209}Bi [15] and ∼10% for ^{9}Be + ^{144}Sm [16] have been reported. The suppression observed in these systems has been understood to be due to the breakup of ^{9}Be leading to loss of flux from the complete-fusion channel. On the other hand, for fusion studies with light mass targets, namely, ^{9}Be + ^{27}Al [17,18] and ^{9}Be + ^{64}Zn [19,20], the TF cross sections have been obtained for the systems, and their comparison with coupled-channels calculations have been reported to show no suppression, with the conclusion that for light systems TF is not affected by the breakup channel. Another explanation has been given by arguing that for these systems, nuclear breakup, which

*ssantra@barc.gov.in

†Present address: Departamento de Física Aplicada, Universidad de Huelva, E-21071 Huelva, Spain.

occurs at short distances, is the dominant process and thus does not inhibit the fusion process [10,17]. To investigate this, exclusive breakup measurement for the ^{9}Be + ^{208}Pb system [21] was carried out with the conclusion, contrary to the above explanation for light systems, that breakup of ^{9}Be in the presence of the heavy target is due to nuclear surface interactions.

With an aim to investigate whether suppression of fusion cross section can be found for ^{9}Be induced fusion in a medium mass target in the region $A = 80$–100, we have studied the fusion reaction for the ^{9}Be + ^{89}Y system. The target ^{89}Y was chosen because of the following advantages: (i) it being a neutron magic nucleus ($N = 50$), the effect of coupling of the target inelastic states would be less than that for a deformed target, making it easy to single out the effect of breakup coupling, (ii) it is monoisotopic, thus contribution to the same evaporation residues (ERs) formed from other isotopes is avoided, (iii) fusion of ^{89}Y with ^{9}Be forms the compound nucleus (CN) ^{98}Tc, and the ERs formed due to particle emission have half-lives from a few minutes to a few days, making the offline γ counting measurement possible, and (iv) the study of isotopes of technetium has additional interest due to their use in medical and industrial applications.

Two other fusion measurements, involving tightly bound projectiles, have been carried out for the ^{4}He + ^{93}Nb and ^{12}C + ^{89}Y systems. Both systems form a CN nearby to ^{98}Tc. The CF cross sections obtained for these systems have been compared with the corresponding values for ^{9}Be + ^{89}Y to establish the observed suppression in the system. It must be mentioned here that for the ^{4}He + ^{93}Nb system, individual ER cross sections at few energies are already available in the literature. However, fusion cross sections extracted from these measurements do not show a smooth variation with energy. Hence, fusion measurement for this system was repeated.

In a recent systematic study [22] involving weakly bound stable projectiles and heavy targets, the complete fusion fraction, $F_{\rm CF}$, was plotted as a function of Z_pZ_t. For fusion of ^{6,7}Li and ^{10,11}B projectiles, this fraction was found to be independent of Z_pZ_t within their experimental errors. However, for the ^{9}Be induced fusion, $F_{\rm CF}$ shows variation, indicating its target dependence. With the addition of the current result, a discussion regarding this observation is presented for ^{9}Be induced fusion.

The paper is organized as follows. Experimental details for all the measurements are given in Sec. II. Data analysis is described in Sec. III. This section is further divided into five subsections. In Sec. III A, the details of the ERs observed in all three measurements are given. In Sec. III B, details regarding the extraction of experimental fusion cross sections, barrier distribution, and comparison of the cross sections with statistical model calculations for the ^{9}Be + ^{89}Y system are given. Coupled-channels calculations are described in Sec. III C. Section III D compares the cross sections for the ^{9}Be + ^{89}Y system with those for ^{4}He + ^{93}Nb and ^{12}C + ^{89}Y systems. A discussion on the CF suppression factor for reactions induced by ^{9}Be on different mass targets is given in Sec. III E. A summary of the study and conclusions from the analysis are found in Sec. IV.

II. EXPERIMENTAL DETAILS

Fusion studies for all three systems were carried out using the 14UD BARC-TIFR Pelletron Accelerator facility at Mumbai, India. The offline γ counting method was employed for all measurements. One high-purity germanium (HPGe) detector having an energy resolution of ∼1.7 keV for E_γ = 778 keV and ∼2 keV for E_γ = 1408 keV of the ^{152}Eu standard source was used for this purpose. In all the irradiations, aluminum catcher foils of thickness ∼1 mg/cm^2 were used along with each target foil to stop the recoiling ERs. To monitor current variations during each irradiation, a CAMAC scaler was utilized which recorded the integrated current in intervals of 1 min. Energy calibration as well as efficiency of the detector were obtained using the ^{152}Eu and ^{133}Ba standard sources.

For the ^{9}Be + ^{89}Y fusion measurement, irradiations of ^{89}Y foils of thickness ∼0.93 mg/cm^2 were carried out using ^{9}Be beam (current ∼45 enA). Irradiation of the targets was done for beam energies from 20–33 MeV in steps of 1 MeV. The irradiation times were of 4 h duration for all energies above the barrier and between 6 and 12 h for below-barrier energies.

The energies used for irradiation in the ^{9}Be + ^{89}Y measurement are in the range $0.82 \leqslant E_{\rm c.m.}/V_b \leqslant 1.36$. Thus the beam energies for ^{4}He + ^{93}Nb and ^{12}C + ^{89}Y fusion measurements were chosen to be in the same range. In the former, ^{93}Nb foils of thickness ∼1 mg/cm^2 each were used for irradiation with a ^{4}He beam. Beam energies in the range 10.5–17 MeV in steps of ∼1–2 MeV were chosen for the irradiations. An average beam current of 28 enA was obtained during the experiment. Irradiation times were between 2 and 4 h for above-barrier energies and between 6 and 7 h for below-barrier energies. For the ^{12}C + ^{89}Y fusion measurement, ^{89}Y foils of thickness ∼1.1 mg/cm^2 each were irradiated with a ^{12}C beam (current ∼160 enA) for energies from 32 to 47 MeV in steps of ∼2 MeV. Irradiation times were between 4 and 6 h for above-barrier energies and 7–9 h for below-barrier energies.

III. ANALYSIS

A. Details of the evaporation residues formed in the systems studied

The fusion of ^{9}Be with ^{89}Y forms the CN ^{98}Tc in an excited state which then deexcites mainly by neutron evaporation to lower A isotopes of Tc. None of these isotopes are stable and they decay mainly by electron capture. The dominant channels measured in the experiment include $2n$ and $3n$ evaporation (∼80–90% of $\sigma_{\rm fus}$ as estimated from the statistical model code PACE [23]) giving the ERs ^{96}Tc and ^{95}Tc, respectively. Other ERs observed are ^{94}Tc ($4n$ evaporation), ^{92}Nb ($\alpha 2n$-CF/$1n$-α ICF) and ^{90}Y ($1n$ transfer). The unmeasured ERs include ^{96}Mo (pn evaporation) and ^{95}Mo ($p2n$ evaporation) which constitute about 10–20% of the $\sigma_{\rm fus}$. These ERs are stable and thus could not be measured using the offline counting method. Table I shows the measured ERs of the above reaction along with those for the ^{4}He + ^{93}Nb and ^{12}C + ^{89}Y systems, corresponding evaporation channels, half-lives, γ energies, and their absolute intensities.

TABLE I. Evaporation residues identified in the three measurements along with their half-lives $T_{1/2}$, E_γ, and their absolute intensities I_γ. The first column is divided into three parts according to the reaction studied and gives the evaporation channels for the corresponding reaction mentioned in the title.

^{9}Be + ^{89}Y	Reaction ^{12}C + ^{89}Y	^{4}He + ^{93}Nb	Residue	$T_{1/2}$	E_γ (keV)	I_γ (%)
$2n$	αn	$1n$	$^{96}_{43}$Tc^{g}	4.28 d	812.54	82
					1126.85	15.2
$2n$	αn	$1n$	$^{96}_{43}$Tc^{m}	51.5 min	1200.15	1.1
$3n$	$\alpha 2n$	$2n$	$^{95}_{43}$Tc^{g}	20 h	765.79	93.8
					1073.71	3.74
					947.67	1.95
$3n$	$\alpha 2n$	$2n$	$^{95}_{43}$Tc^{m}	61 d	835.15	26.6
$4n$	–	–	$^{94}_{43}$Tc^{g}	293 min	702.67	99.6
					916.10	7.6
$4n$	–	–	$^{94}_{43}$Tc^{m}	52 min	1522.1	4.5
$\alpha 2n$-CF/	–	–	$^{92}_{41}$Nb^{m}	10.15 d	934.44	99.1
$1n$-α ICF						
$1n$	–	–	$^{90}_{39}$Y	3.19 h	202.53	97.3
Transfer					479.51	90.7
–	$2n$	–	$^{99}_{45}$Rh^{g}	4.7 h	340.8	70
–	$2n$	–	$^{99}_{45}$Rh^{m}	16.1 d	353.05	34.6
–	$3n$	–	$^{98}_{45}$Rh^{g}	8.72 min	652.6	97
					761.5	1.11
–	$3n$	–	$^{98}_{45}$Rh^{m}	3.6 min	652.6	96
					745.2	78
–	$4n$	–	$^{97}_{45}$Rh^{g}	30.7 min	840.13	12.0

Fusion of ^{4}He + ^{93}Nb forms the CN ^{97}Tc which decays mainly (via electron capture) by $1n$ and $2n$ evaporation (~98% of $\sigma_{\rm fus}$ from PACE) to give the ERs ^{96}Tc and ^{95}Tc, respectively. The remaining ~2% of the fusion cross sections consist of ^{96}Mo ($1p$ evaporation), ^{95}Mo (pn evaporation) and ^{93}Nb (α evaporation) which are stable ERs. Fusion of ^{12}C + ^{89}Y forms the CN ^{101}Rh which decays mainly (via electron capture and β^+) by the $2n$ (^{99}Rh), $3n$ (^{98}Rh), αn (^{96}Tc), and $\alpha 2n$ (^{95}Tc) evaporation channels (for details of ERs see Table I) which form about 90% of the total fusion cross section. The remaining ~10% of the cross section consists of ^{99}Ru (pn evaporation) and ^{98}Ru ($p2n$ evaporation), which are stable ERs.

Figure 1 shows a typical γ-ray spectrum obtained after 4 h of irradiation of the ^{89}Y target with ^{9}Be beam at $E_{\rm lab}$ = 32 MeV, where the γ lines of interest are clearly identified. To confirm that the γ lines observed are coming from the ERs of interest, the half-life for each ER has been followed (the same procedure has been applied for the γ lines obtained in the other two experiments). Figure 2 shows the half-lives followed for two of the ERs. The solid lines are decay curve fits to the experimental data points using literature values [24] for the half-lives.

B. Fusion cross sections and barrier distribution for the ^{9}Be + ^{89}Y system

The experimental ER cross sections for the system were obtained using the formula

$$\sigma_{\rm ER}^{\rm expt} = \frac{Y\lambda}{N_t \epsilon I_\gamma (1 - e^{-\lambda t_{\rm step}})k}, \qquad (1)$$

where

$$k = \sum_{n=1}^{m} I_n (e^{-\lambda[t_1+(n-1)t_{\rm step}]} - e^{-\lambda[t_2+(n-1)t_{\rm step}]}). \qquad (2)$$

In Eq. (1), Y is the yield of the γ line of interest; λ, the disintegration constant of the ER; N_t, target thickness; ϵ, efficiency of the detector for the γ line; I_γ, absolute intensity of the γ line; t_1 and t_2, counting times of the irradiated samples; and $t_{\rm step}$, step size in which the current was recorded in the

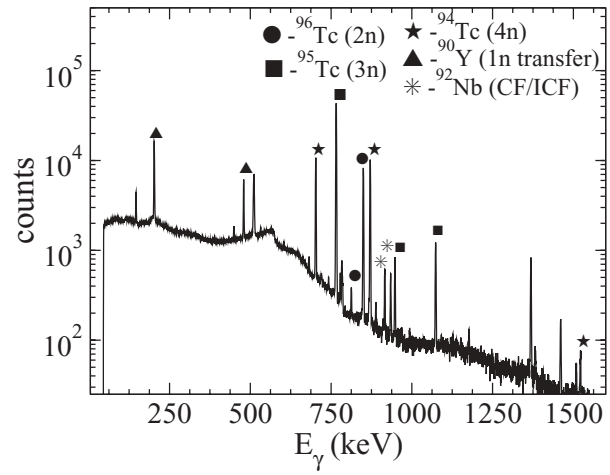

FIG. 1. Typical γ-ray spectrum obtained after 4 h of irradiation of ^{89}Y target with ^{9}Be beam at $E_{\rm lab}$ = 32 MeV. The γ lines from ERs of interest have been marked by symbols on top of the respective peaks.

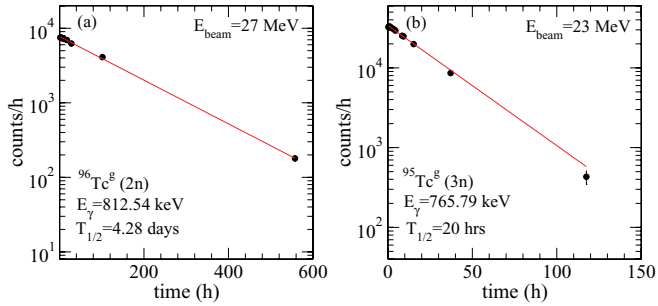

FIG. 2. (Color online) Decay curves for the ER (a) $^{96}\mathrm{Tc}^{g}$ with $E_\gamma = 812.54$ keV at $E_{\mathrm{beam}} = 27$ MeV and (b) $^{95}\mathrm{Tc}^{g}$ with $E_\gamma = 765.79$ keV at $E_{\mathrm{beam}} = 23$ MeV.

scaler. In Eq. (2), I_n is the current recorded by the scaler at the nth interval and m is the total number of intervals. The values for each σ_{ER} thus obtained are plotted in Fig. 3. The $1n$ transfer (^{90}Y) channel cross sections have been plotted in Fig. 4.

The measured ER cross sections have been compared with statistical model calculations performed using the code PACE. The l distribution obtained from the coupled-channels code CCFULL [25] was given as an input at each energy to obtain the cross sections. A level density parameter of $A/9.6$ MeV^{-1} was used for the calculations. This value was chosen because it reproduced the ratio σ_{3n}/σ_{2n}, of the two dominant channels observed. The ER cross sections thus obtained are plotted in Fig. 3 as dotted line for ^{96}Tc, dashed line for ^{95}Tc, dot-dashed line for ^{94}Tc, and solid line for ^{92}Nb. The unaccounted cross sections, due to the formation of stable ERs in the reaction, were accounted for from PACE by taking the ratio $R = \sum_x \sigma_{xn}^{\mathrm{PACE}}/\sigma_{\mathrm{fus}}^{\mathrm{PACE}}$ where $x = 2, 3, 4$ and using this ratio to calculate the CF cross sections by $\sigma_{\mathrm{fus}}^{\mathrm{expt}} = \sum_x \sigma_{xn}^{\mathrm{expt}}/R$. The CF cross sections are plotted in Fig. 5(a) as filled circles. The values of the ratio R and the fusion cross sections are given in Table II. The energies mentioned in the first column

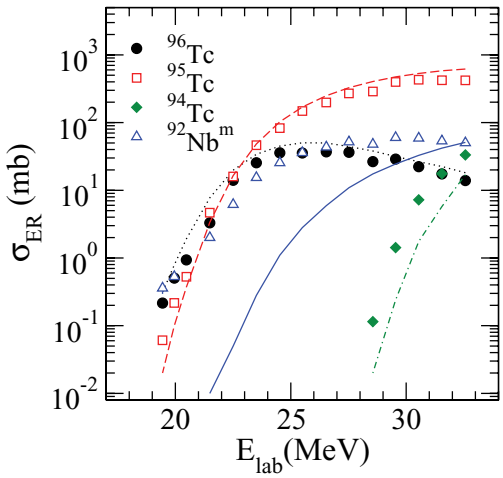

FIG. 3. (Color online) Experimental ER cross sections, obtained in the $^{9}\mathrm{Be} + ^{89}\mathrm{Y}$ fusion measurement, as a function of the projectile laboratory energy. Results from the statistical model calculations for the corresponding ERs are shown by dotted line (^{96}Tc), dashed line (^{95}Tc), dot-dashed line (^{94}Tc), and solid line (^{92}Nb).

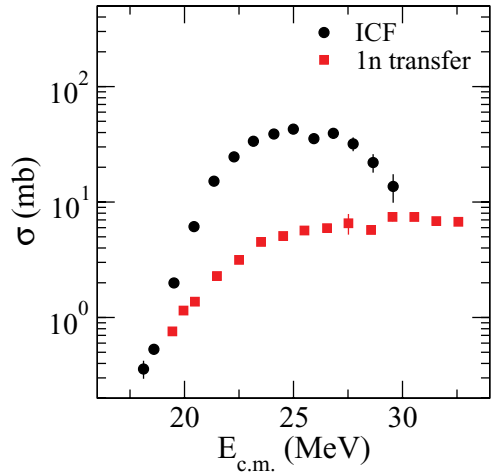

FIG. 4. (Color online) ICF and the $1n$ transfer cross sections as a function of $E_{\mathrm{c.m.}}$ obtained in the $^{9}\mathrm{Be} + ^{89}\mathrm{Y}$ fusion reaction.

are those obtained after correcting for the energy loss at half the target thickness. Errors on the cross sections were estimated by taking into account errors in yield (∼2%), absolute intensity

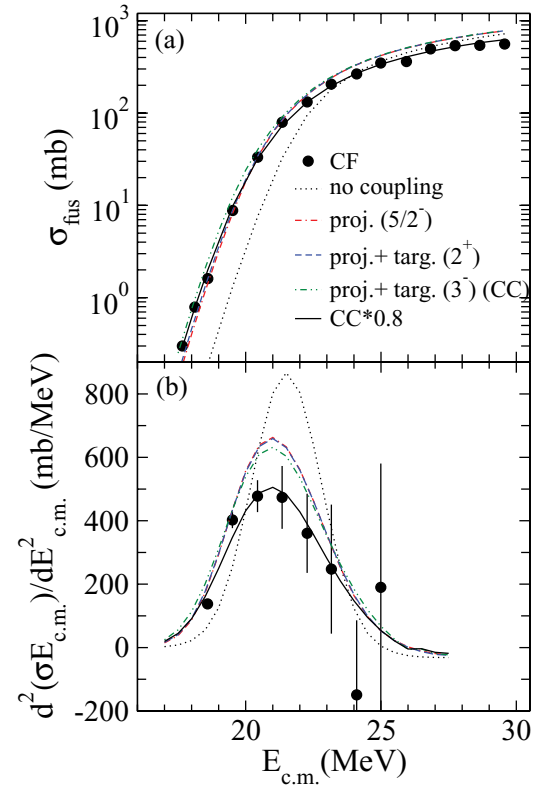

FIG. 5. (Color online) (a) Experimental fusion cross sections (filled circles) along with those obtained without coupling (dotted line), projectile coupling only (dot-dash line), projectile + target 2^+ excited state coupling (dashed line), and projectile + target 3^- excited state (CC calculations) coupling (dot-dot-dash). The solid line represents the cross sections obtained after multiplication of the CC results by a factor of 0.80. (b) Corresponding barrier distribution obtained from the experimental cross sections (filled circles) as well as the coupling introduced as mentioned in the text.

TABLE II. Experimental fusion cross sections along with the ratio R (see text for definition).

$E_{\rm lab}$ (MeV)	$E_{\rm c.m.}$ (MeV)	R	$\sigma_{\rm fus}^{\rm expt}$(mb)
19.4	17.7	0.9167	0.30 ± 0.03
19.9	18.1	0.9175	0.78 ± 0.06
20.5	18.6	0.9120	1.6 ± 0.1
21.5	19.5	0.9054	8.8 ± 0.5
22.5	20.4	0.9049	33.2 ± 1.9
23.5	21.3	0.9021	79.6 ± 4.1
24.5	22.3	0.8988	132 ± 7
25.5	23.2	0.8929	206 ± 13
26.5	24.1	0.8871	265 ± 14
27.5	24.9	0.8802	348 ± 20
28.6	25.9	0.8717	361 ± 20
29.5	26.8	0.8650	495 ± 35
30.5	27.7	0.8559	537 ± 31
31.5	28.6	0.8453	541 ± 33
32.6	29.8	0.8367	559 ± 32

of the γ line ($\sim$4%), target thickness ($\sim$2%), and efficiency of the detector for that γ line ($\sim$3%).

From Fig. 3, it can be seen that the experimental values of the individual ERs match well with the corresponding PACE values except for ^{92}Nb (unfilled triangles) which has contributions from both CF and ICF channels. Thus the ICF cross section was estimated by subtracting the PACE results for the ^{92}Nb ER from the experimental ^{92}Nb^{m} cross sections at each energy. The values thus obtained are plotted in Fig. 4. We consider this as a lower limit of the ICF cross section, because when the CN decays to give the ^{92}Nb ER, some of the CN decay will also populate ^{92}Nb^{g}. This ER could not be measured by the offline counting method, employed for the current investigation, due to its long half-life (3.47×10^{7} yr).

From the experimental fusion cross sections, $\sigma_{\rm fus}^{\rm expt}$, a distribution of fusion barriers has been extracted by taking the second derivative of the product $E_{\rm c.m.}\sigma_{\rm fus}^{\rm expt}$ with respect to $E_{\rm c.m.}$ following the procedure given in Ref. [26]. The results are shown in Fig. 5(b) as filled circles. To obtain the average fusion barrier, a weighted average of the barriers was taken with the weights given by $d^2 E_{\rm c.m.}\sigma_{\rm fus}^{\rm expt}/dE_{\rm c.m.}^2$ at each barrier energy. An average barrier of $V_b = (21.8 \pm 0.3)$ MeV was found using this procedure.

C. Coupled-channels calculations

To study the effect of coupling on fusion cross sections, CC calculations were performed using a modified version of CCFULL [25] in which coupling to the projectile excited states

TABLE III. Coupling parameters used in the CC calculations.

Nucleus	J^{π}	E_x (MeV)	β
^{9}Be	$3/2^{-}$	0.000	1.300
	$5/2^{-}$	2.429	0.720
^{89}Y	2^{+}	2.011	0.104
	3^{-}	2.742	0.208

TABLE IV. Potential parameters used for the ^{9}Be + ^{89}Y, ^{4}He + ^{93}Nb, and ^{12}C + ^{89}Y systems along with the barrier height V_b, barrier radius R_b, and barrier curvature $\hbar\omega$.

System	Potential	V_o (MeV)	r_o (fm)	a_o (fm)	V_b (MeV)	R_b (fm)	$\hbar\omega$ (MeV)
^{9}Be + ^{89}Y	AW	43.99	1.17	0.63	21.48	9.76	3.90
	CC	55.00	1.11	0.69	21.60	9.63	3.76
^{4}He + ^{93}Nb	AW	32.16	1.14	0.63	11.38	9.18	4.31
^{12}C + ^{89}Y	AW	49.58	1.18	0.63	31.83	9.88	4.10

and the effect of the projectile ground-state spin are included. Projectile couplings to the ^{9}Be ground state, $J^{\pi} = 3/2^{-}$, with deformation parameter $\beta = 1.3$ [27], and the $5/2^{-}$ excited state in its ground-state rotational band (band head $K = 3/2^{-}$) with $E_x = 2.429$ MeV, $\beta = 0.72$ [28] were included. Target inelastic states have also been coupled in the calculations. To include the effects of target excitations within the limited model space of CCFULL, the effects of the multiplets have been incorporated in a single vibrational state (2^{+} or 3^{-}) by taking the average of the excitation energy and deformation parameter corresponding to the neighboring even-even nuclei, namely, ^{88}Sr and ^{90}Zr, as done in Ref. [29]. The excitation energies and deformation parameters of different inelastic states of ^{9}Be and ^{89}Y that have been used in the CC calculations are given in Table III. The Woods-Saxon parametrization of the Akyuz-Winther (AW) potential [30] was utilized to get the initial input potential parameters for CCFULL (see Table IV for values). After introducing the couplings, the potential parameters were varied so as to reproduce the experimental average barrier V_b obtained as mentioned in Sec. III B. This could be achieved for $V_o = 55$ MeV, $r_o = 1.11$ fm, and $a_o = 0.69$ fm, which gives $V_b = 21.6$ MeV, $R_b = 9.63$ fm, and $\hbar\omega = 3.76$ MeV. The results thus obtained are shown in Fig. 5(a). Here the dotted line represents the cross sections obtained without coupling, the dot-dashed line represents the cross sections obtained when coupling to only the projectile excited ($5/2^{-}$) state is included, the dashed line represents cross sections obtained by coupling the projectile excited ($5/2^{-}$) state and the 2^{+} excited state of the target, and the dot-dot-dashed line represents the cross sections obtained by coupling the projectile excited ($5/2^{-}$) state and the 3^{-} excited state of the target (CC). Figure 5(b) shows the corresponding barrier distributions. It can be seen from the figure that the effect of coupling to the 2^{+} excited state of the target on the fusion cross sections and barrier distributions is negligible compared to that of the 3^{-} state. Thus, in the final calculations, coupling to only the 3^{-} state was included for the target coupling. From the figure it can also be seen that the fusion cross sections obtained from the CC calculations with the above couplings are higher than the experimental values especially at above-barrier energies, indicating a suppression in measured CF cross sections for the ^{9}Be + ^{89}Y. Multiplication of the CC results by the factor 0.80, shown by the solid line in Fig. 5(a), is able to reasonably reproduce the measured CF cross sections. This implies that the measured CF cross sections are suppressed by 20% compared to the values predicted by the above model.

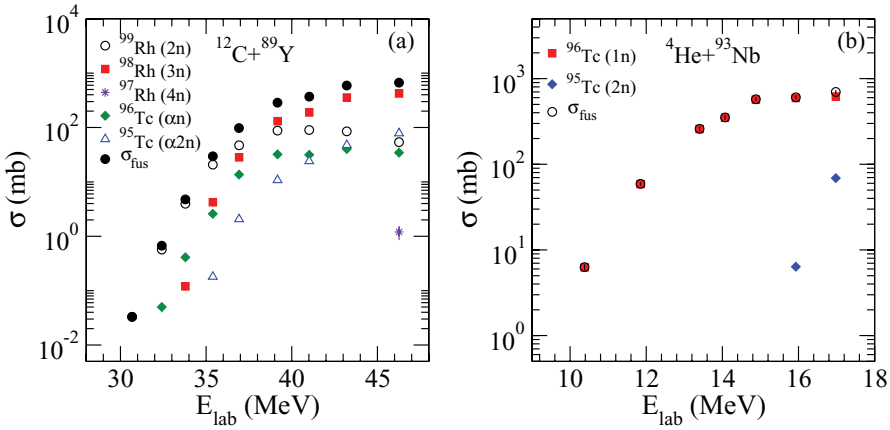

FIG. 6. (Color online) Experimental ER cross sections along with the TF cross section as a function of laboratory energy of the projectile for (a) $^{12}C + ^{89}Y$ and (b) $^{4}He + ^{93}Nb$ systems.

D. Comparison with $^{4}He + ^{93}Nb$ and $^{12}C + ^{89}Y$ systems

Fusion cross sections for the $^{4}He + ^{93}Nb$ and $^{12}C + ^{89}Y$ systems were obtained following the same procedure as that mentioned in Sec. III B. The experimental ER cross sections as well as the total fusion cross sections for both the systems are plotted in Fig. 6. For comparing the cross sections for $^{9}Be + ^{89}Y$ with these two systems, two reduction procedures were used. In the first method, the reduced fusion cross section, $\sigma_{fus}/\pi R_b^2$, was plotted as a function of the center-of-mass energy normalized to barrier, $E_{c.m.}/V_b$, as shown in Fig. 7(a). In the second procedure, the geometrical dependence is eliminated in an approximate way [31] by taking $R_b = r_o(A_p^{1/3} + A_t^{1/3})$ and $V_b = Z_p Z_t e^2/R_b$. Thus in Fig. 7(b), $\sigma_{fus}/(A_p^{1/3} + A_t^{1/3})^2$ versus $E_{c.m.}(A_p^{1/3} + A_t^{1/3})/Z_p Z_t$ has been plotted. In both the figures, the dotted line represents the cross sections obtained from the CC calculations for the $^{9}Be + ^{89}Y$ which have been reduced according to the two procedures mentioned, respectively, and the solid lines are the corresponding values after multiplication by 0.8. In the former reduction method, the Woods-Saxon parametrization of the AW potential was utilized to obtain the values of V_b and R_b for the latter two systems. The potential parameters utilized for all three systems and the corresponding barrier height, barrier radius, and curvature obtained from them are summarized in Table IV.

Since the CN formed by the three systems are similar, one would expect the cross sections to overlap at above-barrier energies where the effect of coupling of bound inelastic states and transfer states are supposed to be negligible. However, as can be seen from Figs. 7(a) and 7(b), the reduced cross sections, obtained from both reduction procedures, for the $^{4}He + ^{93}Nb$ and $^{12}C + ^{89}Y$ system are larger than the corresponding values for the $^{9}Be + ^{89}Y$ system. Further, the CC cross sections have to be multiplied by a factor of 0.80 ± 0.05 to obtain a reasonable reproduction of the experimental cross sections for $^{9}Be + ^{89}Y$ system. This again indicates that the CF cross sections for the $^{9}Be + ^{89}Y$ system are suppressed by $(20 \pm 5)\%$, which further supports our conclusion of suppression for the system. The error on the multiplication factor was taken as its deviation from the value of 0.80 which could still reproduce the experimental barrier distribution.

E. Suppression factors for ^{9}Be induced fusion reactions

We discuss here the systematics for the CF suppression factors obtained in case of ^{9}Be induced fusion reactions with different mass targets. From the current measurement for the $^{9}Be + ^{89}Y$ system, the suppression in CF cross sections has surprisingly been found to be more than that for the fusion with a heavier target in the $^{9}Be + ^{144}Sm$ reaction. However, a recent study of systematics of the breakup in reactions of ^{9}Be at near-barrier energies [32] found that the ratio of the suppression factor to the ICF is independent of Z_t, and the probability of ICF increases with Z_t. Accordingly, the suppression factor for the present system should have

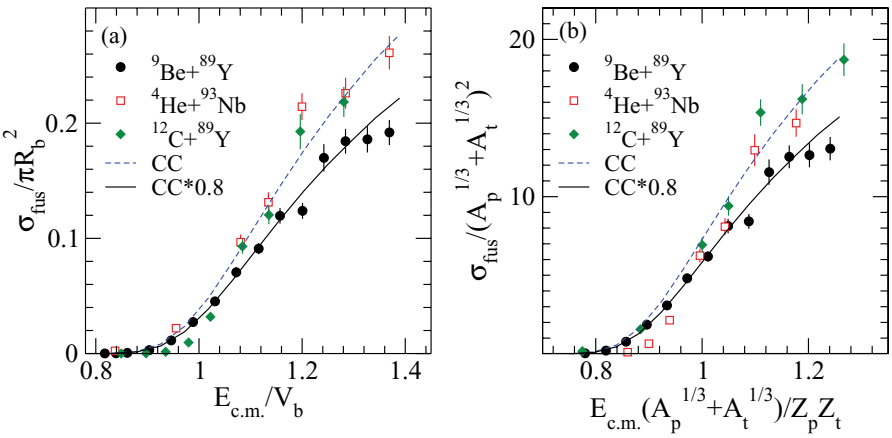

FIG. 7. (Color online) Reduced cross sections for the $^{9}Be + ^{89}Y$ system compared with those for $^{4}He + ^{93}Nb$ and $^{12}C + ^{89}Y$ systems using the two reduction procedures as mentioned in the text. In both figures, the dashed line represents the cross sections obtained from the CC calculations for the former system, while the solid line represents the CC cross sections after multiplication by 0.80.

been smaller than for ^{9}Be + ^{144}Sm, contrary to the present observation. There have also been recent calculations [33] done to estimate the suppression factors for ^{9}Be + ^{144}Sm and ^{9}Be + ^{208}Pb systems. For the former case, the CF suppression of 10% has been obtained by adding an adjustable repulsive part (which simulates the effect of nuclear incompressibility) of the effective *NN* interaction that is used in the calculation of the double-folding nuclear potential. Using the same value of the repulsive potential for the ^{9}Be + ^{208}Pb system, a suppression of 20% in CF was predicted, which underestimates the observed suppression (∼30%) in Ref. [14]. By comparing the suppression factor for the present target with ^{208}Pb and ^{209}Bi, one can suggest that the actual strength of the repulsive potential is higher than the one used in Ref. [33], and this leads to the conclusion that the suppression factor observed for ^{144}Sm is less than expected. Since the coupling of the breakup channels is known to generate a repulsive term to the effective interaction, an additional strength may be necessary other than the nuclear incompressibility to reproduce the observed suppression in measured CF for all the systems.

IV. SUMMARY AND CONCLUSIONS

To summarize, we have obtained the fusion excitation function for the ^{9}Be + ^{89}Y system for energies around the Coulomb barrier. Experimental barrier distribution for the system has been extracted from the fusion data and used to find the average barrier height for the system as well as understand the influence of coupling. Simplified coupled-channel calculations have been carried out in which coupling of inelastic channel to fusion has been considered. A lower limit of the α-ICF cross section has also been obtained. Fusion cross sections for the ^{4}He + ^{93}Nb and ^{12}C + ^{89}Y systems have been measured to find any difference in fusion induced by weakly bound and tightly bound projectiles. Systematics of the suppression observed in the ^{9}Be induced reactions on different mass targets has been discussed.

It has been found that the experimental CF cross sections for the ^{9}Be + ^{89}Y system are suppressed by (20 ± 5)% compared to the cross sections predicted by the CC calculations, especially at above-barrier energies. This suppression can be expected to be due to the breakup of the projectile whose effect is not included in the CC calculation. Comparison of the experimental cross sections for ^{9}Be + ^{89}Y with ^{4}He + ^{93}Nb and ^{12}C + ^{89}Y further confirms our observation of CF suppression in the former, because the reduced cross sections for the system are indeed suppressed compared to the latter. Furthermore, a considerable ICF cross section found for the ^{9}Be + ^{89}Y system is a manifestation of loss of incident flux from the CF channel due to the breakup of ^{9}Be, thus again supporting our conclusion of suppression.

While comparing the suppression factor in CF cross sections for ^{9}Be induced reactions involving different targets, it was interesting to observe that the factor for ^{89}Y is higher than ^{144}Sm, contrary to what one would expect from the calculations in Refs. [32,33]. The experimental and theoretical results on CF cross sections involving ^{89}Y, ^{208}Pb, and ^{209}Bi targets suggest that the suppression factor observed for ^{144}Sm is less than expected.

ACKNOWLEDGMENTS

The authors would like to thank the Pelletron Accelerator staff for smooth operation of the machine during the experiments, the target laboratory staff at TIFR for providing a sufficient number of targets, and Mr. P. Patale for his help during the experiments.

[1] L. F. Canto, P. R. S Gomes, R. Donangelo, and M. S. Hussein, Phys. Rep. **424**, 1 (2006), and references therein.
[2] N. Keeley, R. Raabe, N. Alamanos, and J. L. Sida, Prog. Part. Nucl. Phys. **59**, 579 (2007), and references therein.
[3] A. Mukherjee *et al.*, Phys. Lett. B **636**, 91 (2006).
[4] P. K. Rath *et al.*, Phys. Rev. C **79**, 051601(R) (2009).
[5] A. Pakou *et al.*, Eur. Phys. J. A **39**, 187 (2009).
[6] M. Sinha *et al.*, Eur. Phys. J. A **44**, 403 (2010).
[7] M. Ray *et al.*, Phys. Rev. C **78**, 064617 (2008).
[8] Yu. E. Penionzhkevich *et al.*, Eur. Phys. J. A **31**, 185 (2007).
[9] A. Lemasson *et al.*, Phys. Rev. Lett. **103**, 232701 (2009).
[10] S. B. Moraes *et al.*, Phys. Rev. C **61**, 064608 (2000).
[11] M. Beckerman, Rep. Prog. Phys. **51**, 1047 (1988).
[12] A. B. Balantekin and N. Takigawa, Rev. Mod. Phys. **70**, 77 (1998).
[13] K. Hagino, A. Vitturi, C. H. Dasso, and S. M. Lenzi, Phys. Rev. C **61**, 037602 (2000).
[14] M. Dasgupta *et al.*, Phys. Rev. Lett. **82**, 1395 (1999).
[15] M. Dasgupta, D. J. Hinde, S. L. Sheehy, and B. Bouriquet, Phys. Rev. C **81**, 024608 (2010).
[16] P. R. S. Gomes *et al.*, Phys. Rev. C **73**, 064606 (2006).
[17] R. M. Anjos *et al.*, Phys. Lett. B **534**, 45 (2002).
[18] G. V. Martí *et al.*, Phys. Rev. C **71**, 027602 (2005).
[19] P. R. S. Gomes *et al.*, Phys. Lett. B **601**, 20 (2004).
[20] P. R. S. Gomes *et al.*, Phys. Rev. C **71**, 034608 (2005).
[21] D. J. Hinde, M. Dasgupta, B. R. Fulton, C. R. Morton, R. J. Wooliscroft, A. C. Berriman, and K. Hagino, Phys. Rev. Lett. **89**, 272701 (2002).
[22] L. R. Gasques, D. J. Hinde, M. Dasgupta, A. Mukherjee, and R. G. Thomas, Phys. Rev. C **79**, 034605 (2009).
[23] A. Gavron, Phys. Rev. C **21**, 230 (1980).
[24] [http://www.nndc.bnl.gov/chart/].
[25] K. Hagino, N. Rowley, and A. T. Kruppa, Comput. Phys. Commun. **123**, 143 (1999); K. Hagino (private communication).
[26] M. Dasgupta, D. J. Hinde, N. Rowley, and A. M. Stefanini, Annu. Rev. Nucl. Part. Sci. **48**, 401 (1998).
[27] H. J. Votava, T. B. Clegg, E. J. Ludwig, and W. J. Thompson, Nucl. Phys. A **204**, 529 (1973).
[28] H. Nguyen Ngoc, M. Hors, and J. Perez-y-Jorba, Nucl. Phys. **42**, 62 (1963).

[29] A. Mukherjee, M. Dasgupta, D. J. Hinde, K. Hagino, J. R. Leigh, J. C. Mein, C. R. Morton, J. O. Newton, and H. Timmers, Phys. Rev. C **66**, 034607 (2002).
[30] R. A. Broglia and A. Winther, *Elastic and Inelastic Reactions*, Heavy Ion Reaction Lecture Notes Vol. I (Benjamin Cummings, Redwood City, CA, 1981), p. 114.
[31] P. R. S. Gomes, J. Lubian, I. Padron, and R. M. Anjos, Phys. Rev. C **71**, 017601 (2005).
[32] R. Rafiei, R. du Rietz, D. H. Luong, D. J. Hinde, M. Dasgupta, M. Evers, and A. Diaz-Torres, Phys. Rev. C **81**, 024601 (2010).
[33] H. Esbensen, Phys. Rev. C **81**, 034606 (2010).